PCCP

Accepted Manuscript

ROYAL SOCIETY OF CHEMISTRY

rsc.li/pccp

View Article Online
DOI: 10.1039/C8CP06196C

View Article Online
DOI: 10.1039/C8CP06196C

Physical Chemistry Chemical Physics

ARTICLE

A fluorescence nanoscopy marker for Corticotropin-Releasing Hormone type 1 receptor: computer design, synthesis, signaling effects, super-resolved fluorescence imaging, and *in-situ* affinity constant in cells.

Received 00th January 20xx,
Accepted 00th January 20xx

DOI: 10.1039/x0xx00000x

www.rsc.org/

Alan M. Szalai[a,b,†], Natalia G. Armando[c,d,†], Federico M. Barabas[a,e,†], Fernando D. Stefani[a,e], Luciana Giordano[a,f], Sara E. Bari[g], Claudio N. Cavasotto[c,†], Susana Silberstein[c,h,†], Pedro F. Aramendía[a,b,†]

Class B G protein-coupled receptors (GPCRs) are involved in a variety of human pathophysiological states. These groups of membrane receptors are less studied than class A GPCRs due to the lack of structural information, delayed small molecule drug discovery, and scarce fluorescence detection tools available. The class B Corticotropin-Releasing Hormone type 1 Receptor (CRHR1) is a key player in the stress response whose dysregulation is critically involved in stress-related disorders: psychiatric conditions (i.e. depression, anxiety, addictions), neuroendocrinological alterations, neurodegenerative diseases. Here, we present a strategy to label GPCRs with a small fluorescent antagonist that permits the observation of the receptor in live cells through stochastic optical reconstruction microscopy (STORM) with 23 nm resolution. The marker, an aza-BODIPY derivative, was designed based on computational docking studies, then synthesized, and finally tested in biological cells. Experiments in hippocampal neurons demonstrate antagonist effects in similar concentrations as the well-established antagonist CP-376395. A quantitative analysis of two color STORM images enabled the determination of binding affinity of the new marker in the cellular environment.

Introduction

Corticotropin-releasing hormone type 1 Receptor (CRHR1) belongs to the class B family of G-protein-coupled receptors GPCRs.[1] GPCRs are the largest group of membrane proteins, targets for about one third of pharmaceutical agents.[2] Structural studies of transmembrane domains (TMDs), that couple GPCR activation to signaling effectors, were delayed for class B members in relation to class A GPCRs. CRHR1 and the glucagon receptor were the first two class B TMD crystal structures solved.[3, 4]

The corticotropin-releasing hormone (CRH) is a 41-aa peptide ligand for CRHR1, crucial in the integration of neuroendocrine, autonomic, and behavioral responses to stress.[5] CRH-activated CRHR1 triggers a variety of cellular responses, leading to cAMP increase and activation of multiple signaling cascades.[6] Dysregulation of the CRH/CRHR1 responses in the central nervous system is related to mood disorders as anxiety and depression,[7] psychiatric conditions that affect about 15% of the population.[8] Knowledge of the subcellular spatial distribution and pathways of CRHR1 in a neuronal cell context appears as key for the understanding of its pathophysiological action.[9]

Fluorescence nanoscopy is becoming the preferred visualization tool to decipher subcellular protein structures, interactions and pathways.[10-12] These techniques rely on

[a] Centro de Investigaciones en Bionanociencias-"Elizabeth Jares-Erijman" (CIBION), CONICET. Godoy Cruz 2390. 1425 Ciudad de Buenos Aires. Argentina
[b] Departamento de Química Inorgánica, Analítica y Química Física. Facultad de Ciencias Exactas y Naturales. Universidad de Buenos Aires. Pabellón 2. Ciudad Universitaria. 1428 Ciudad de Buenos Aires. Argentina.
[c] Instituto de Investigación en Biomedicina de Buenos Aires (IBioBA). CONICET, Partner Institute of the Max Planck Society. Godoy Cruz 2390. 1425 Ciudad de Buenos Aires. Argentina.
[d] Departamento de Ciencia y Tecnología. Universidad Nacional de Quilmes. Roque Sáenz Peña 352. 1876 Bernal. Provincia de Buenos Aires. Argentina
[e] Departamento de Física, Facultad de Ciencias Exactas y Naturales. Universidad de Buenos Aires. Pabellón 1. Ciudad Universitaria. 1428 Buenos Aires. Argentina.
[f] Departamento de Química Orgánica. Facultad de Ciencias Exactas y Naturales. Universidad de Buenos Aires. Pabellón 2. Ciudad Universitaria. 1428 Ciudad de Buenos Aires. Argentina.
[g] Instituto de Química Física de Materiales, Medio Ambiente y Energía (INQUIMAE) CONICET-UBA. Pabellón 2. Ciudad Universitaria. 1428 Ciudad de Buenos Aires. Argentina.
[h] Departamento de Fisiología, Biología Molecular y Celular. Facultad de Ciencias Exactas y Naturales. Universidad de Buenos Aires. Pabellón 2. Ciudad Universitaria. 1428 Ciudad de Buenos Aires, Argentina
† Corresponding authors: susana.silberstein@ibioba-mpsp-conicet.gov.ar, pedro.aramendia@cibion.conicet.gov.ar
FMB present address: Science for Life Laboratory, KTH Royal Institute of Technology, Tomtebodavägen 23A 171 65 Stockholm, Sweden.
CNC present address: Instituto de Investigaciones en Medicina Traslacional (IIMT), CONICET-Universidad Austral. Av. Presidente Perón 1500. B1629AHJ Derqui-Pilar, Argentina.
AMS and NGA contributed equally to this work.

Electronic Supplementary Information (ESI) available: Experimental details and results on computational chemistry, synthetic strategy, spectroscopy and excited state lifetime, and STORM performance of ABP-09, as well as experiments in cells and estimation of the CRHR1-ABP-09 binding. See DOI: 10.1039/x0xx0

View Article Online
DOI: 10.1039/C8CP06196C

Physical Chemistry Chemical Physics

ARTICLE

switching the fluorescent probes between an emissive and one or more non-emissive states. This gives special relevance to the photophysical properties of the fluorophores,[13] whose brightness, contrast, photostability and switching performance determine the achievable spatial resolution.[14] A remarkable recent advance has brought this limit to 1 nm,[15] practically the size of the fluorophore. Ultimately, the achievable resolution of nanoscopy methods is limited by the physical size of the fluorescent label.

Various fluorescent labeling strategies are available to study biomolecules:[16,17] the production of fusion proteins,[18] labeling by post translational modification,[19,20] or the design of a fluorescent ligand for a specific protein.[21] Targeting a particular protein with a small molecule is the most challenging approach because it requires specific design and synthesis, but has a number of advantages: i) it avoids transfection, which allows its direct use in living cells and studies under endogenous cellular protein expression conditions; ii) It enables the application of fluorescence nanoscopy in its full potential.; and iii) it provides more reliable information about protein-protein interactions.

While different fluorescence labeling approaches have been proposed and carried out for GPCRs,[22-25] tagging the antagonist site with small probes appears as an interesting alternative.[22,23,26] In the past few years, small molecule targeting of GPCRs with photoswitchable ligands to remotely control receptor activation have been reported.[27-30] Specifically for CRHR1, there is a variety of high affinity synthetic non-fluorescent antagonists that modulate CRH effects.[8,31-33] One of them, CP-376395, was crystallized with CRHR1.[3]

All these facts encouraged us to design a fluorescent probe for super-resolution fluorescence microscopy that would bind to the antagonist site of CRHR1. Figure 1 summarizes the strategy of this work. First, the structural analysis of effective synthetic antagonists was used to propose fluorescent structures that were analyzed by docking studies. The chosen candidate proved very effective as CRHR1 antagonist and showed excellent features for fluorescence nanoscopy. The fluorophore was used together with fluorescent immunolabeling of CRHR1 to estimate the binding equilibrium constant in neuronal cells by two color stochastic optical reconstruction microscopy (STORM).

Results and Discussion

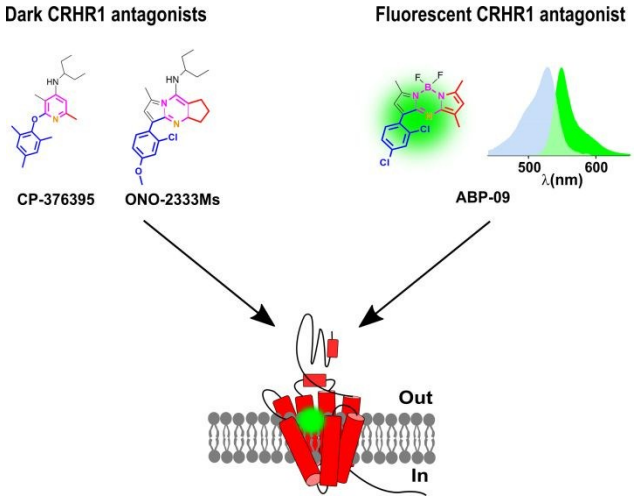

Figure 1: The structure of CP-376395 and ONO-2333MS, synthetic antagonists of CRHR1, inspired the proposal of fluorophore ABP-09 as a ligand for the antagonist site of CRHR1.

Design and synthesis of ABP-09

We selected an aza-BODIPY scaffold as the basis for the fluorescent marker for the well described fluorescent features of this type of compounds, for the versatility of the spectral and photochemical properties, which can be modulated by substitution, and for their photochemical stability.[34,35] We performed in silico docking onto CRHR1 (PDB: 4K5Y) of structures ABP-01 to ABP-11 (see Table S1), compared to the co-crystallized ligand CP-376395 and to ligand ONO-2333Ms[31] as controls. It was implemented with a flexible-ligand--rigid-receptor approach in the ICM software.[36,37] Evident docking difficulty prevents pluri-aromatic substitution in ABPs. This is a strong constraint for aza-BODIPY synthetic feasibility (see below).

Computational chemistry results, combined with photochemical stability criteria, showed that ABP-09 was the best candidate among the proposed structures to act as a stable antagonist for CRHR1, as we explain in what follows. The lowest-energy pose of CP-376395 exhibited a RMSD of 0.4 Å compared to the crystal structure, while ONO-2333Ms pose showed a consistent overlap with it (Figure S9). These two ligands, as well as all ABP proposed structures through its central nitrogen, establish a key H-bond with N283$^{5.50}$ (Wootten numbering shown in superscript[38]). Due to the approximations involved, docking scores may correlate poorly with binding affinities,[39,40] so a

View Article Online
DOI: 10.1039/C8CP06196C

Physical Chemistry Chemical Physics

ARTICLE

simple energy rescoring was performed, using a flexible-ligand—flexible-receptor methodology, similar to the ligand-steered approach,[41-43] but replacing the stochastic sampling by a faster local energy minimization. We omitted the entropic component of the free energy, since only a semi-quantitative estimation of the binding free energy is sought. According to this approach, the binding free energy trend is:

CP-376395<ONO-2333Ms~ABP-09~ABP-11~ABP-10.

Considering the chemical stability provided by the methyl substituents in positions 3 and 5 (Table S1), we chose ABP-09 as the antagonist candidate, among the three best ABP structures. Figure 2 compares the docking of CP-376395 and ABP-09. In ABP-09, the 2,4-dichlorophenyl group occupies the same region as the 2,4,6-trimethylphenyl group of CP-376395.

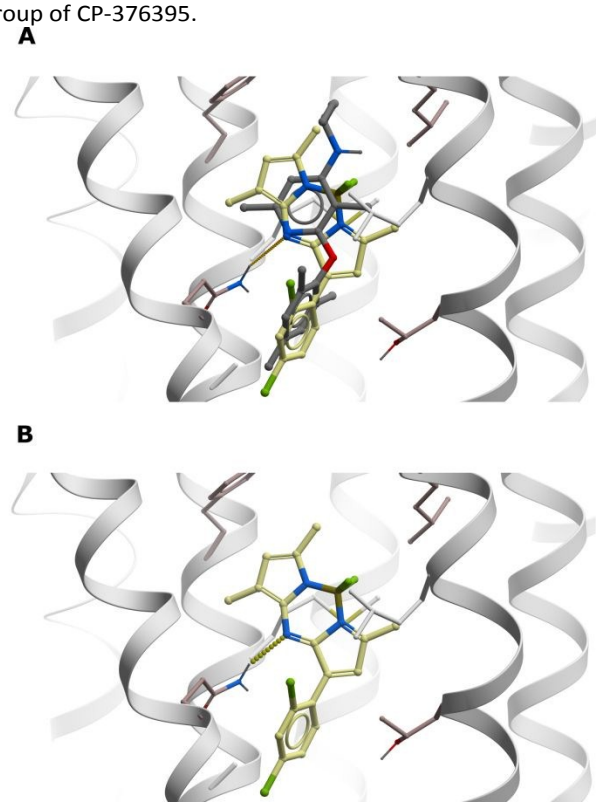

Figure 2. A) Docking of CP-376395 (grey carbons) and ABP-09 (light yellow carbons). B) Docking of ABP-09. Dotted lines display the H-bond to N283$^{5.50}$. CRHR1 helices are displayed as light grey ribbons, and key interacting amino-acids as sticks. Color code: grey, carbon; blue, nitrogen; red, oxygen; green: chlorine. (Figure prepared with ICM, Molsoft LLC).

The synthetic route for ABP-09 is depicted in Figure 3. The pathway was designed taking advantage of the intrinsically asymmetric reaction mechanism,[44,45] and avoiding the isolation of an unstable α–nitroso pyrrole intermediate.

As almost all aza-BODIPYs described are tetra aryl substituted,[44,46] the synthesis of the ABP-09 posed a challenge. The overall yield of ABP-09 is less than 1% starting from compound **2**, but upon isolation this new compound was thermally and photochemically stable.

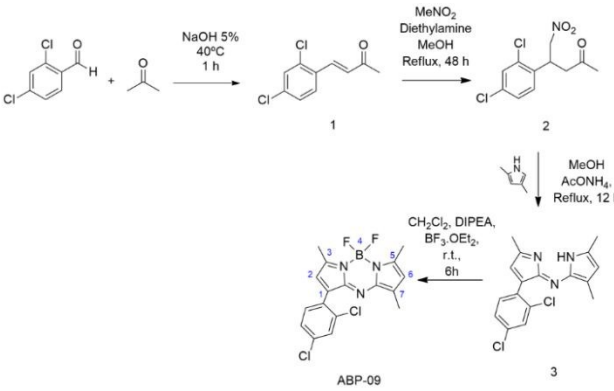

Figure 3 Synthetic route for ABP-09.

Spectroscopic properties of ABP-09

The absorption coefficient ε_{530}= (70 ± 10) 10^3 M^{-1} cm^{-1}, was derived by comparison to BODIPYs and aza-BODIPYs of similar structure and energy.[47-50]

ABP-09 displays a moderate negative solvatochromism. The energy of the maximum absorption and emission wavelength as well as the Stokes shift show a linear dependence with the $E_T(30)$ solvent parameter, as displayed in Figure S10. Absorption and emission maxima are located at 535 and 552 nm in toluene, at 529 and 550 nm in dichloromethane (see Figure 4A), at 517 and 544 in acetonitrile, and at 518 and 546 nm in methanol, respectively (Figure S10). Most BODIPY compounds show a very mild positive solvatochromism that is greatly enhanced when electron donating and withdrawing substituents.[51] Interestingly, a recent work reports the negative solvatochromism of a group of push-pull aza-BODIPYs with the same substitution pattern in both indole rings.[52] The magnitude of the solvatochromic shift in absorption between toluene and acetonitrile is similar to ABP-09, a compound that has moderate electron attracting and donating groups in only one ring.

View Article Online
DOI: 10.1039/C8CP06196C

Physical Chemistry Chemical Physics

ARTICLE

The red shift (>35nm) in the maximum absorption wavelength of ABP-09 as compared to the 1,3,5,7-methyl substituted BODIPY[53] is a consequence of the aza-BODIPY structure. Indeed, such a red-shifted absorbance cannot be explained in terms of an extended conjugation introduced by the 2,4-dichlorophenyl substituent in position 1. This statement is based on the electron withdrawing properties of the chlorine atoms present in the substituent and the low impact of substituents in position 1 to bathochromic shifts.[51,53,54] Taken together, these considerations support that the observed red shift is a consequence of the effect of the N atom in the *meso* position.[51,55]

The emission in dichloromethane has a quantum yield of 0.86 ± 0.04, and a lifetime of 3.84 ± 0.01 ns (λ_{exc} = 490 nm, Figure 4B).

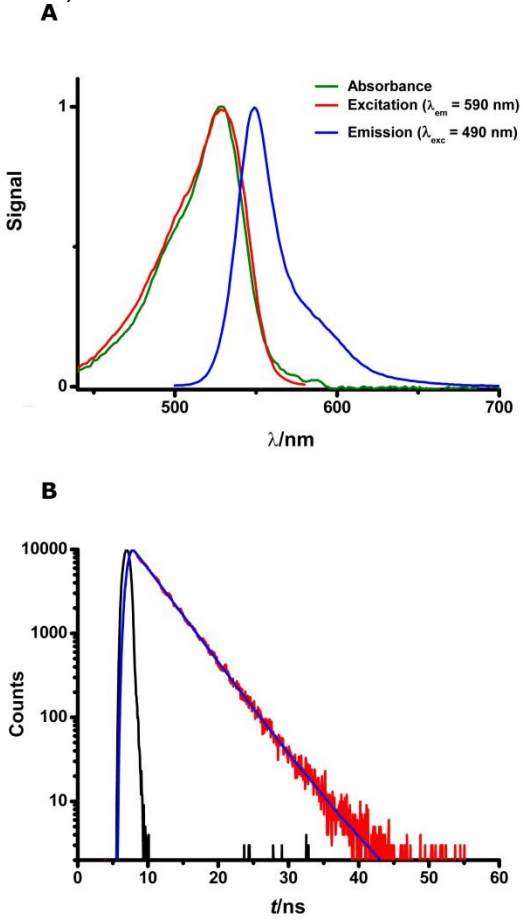

Figure 4. A) Absorption (green line) and fluorescence emission (blue line, λ_{exc} = 490 nm) and excitation (red line, λ_{em} = 590 nm) spectra of ABP-09 in DCM. Spectra are normalized to their respective maximum. B) Emission decay in DCM. Black line: Instrument response function (IRF). Red line: experimental decay. Blue line: Fit to the data of a convolution of a monoexponential decay with 3.84 ± 0.01 ns and the IRF.

ABP-09 and CP-376395 effect on CRH-activated CRHR1 signaling

The influence of ABP-09 and the CRHR1 antagonist CP-376395 in signaling effectors downstream CRH-activated CRHR1 was tested in HT22-CRHR1 and in HT22-CRHR1-Epac-S^{H187} cells, stably expressing CRHR1 and both CRHR1 and the FRET-based biosensor for cAMP Epac-S^{H187}, respectively (see Materials and Methods and SI).[56] First, using HT22-CRHR1-Epac-S^{H187} cells, 10 nM CRH stimulation triggered a rapid and sustained cAMP response (Figure 5) as previously reported.[56] In cells preincubated with either ABP-09 or the antagonist CP-376395 in 10 or 100 nM concentration, cAMP levels decreased similarly compared to control conditions (Figure 5). The preincubation used before stimulation was 20 h, time after which ABP-09 concentration in living cells attains a level independent of the initial dose that remains constant in time (see Materials and Methods and Figure S12). For both species, the 50% decrease in the FRET response demonstrates an inhibiting effect in this CRHR1 signaling pathway with comparable effectiveness for ABP-09 and CP-376395, showing saturation effect at 10 nM concentration added.

Further evidence of ABP-09 antagonist action was obtained from the analysis of the activation (phosphorylation) of signaling proteins downstream stimulated CRHR1. Cells were also preincubated during 20 h with ABP-09 in these experiments. Two phosphoprotein levels were assessed by Western Blot in HT22-CRHR1 cells stimulated with 100 nM CRH: pERK1/2, monitored 5 minutes after stimulation and pAkt, monitored 30 minutes after stimulation[57] Whereas no effects were observed in basal phosphoprotein levels, when either 100 nM or 1 μM ABP-09 was present there was a decrease to 75% of the maximum response in pERK1/2 after 5 minutes of stimulation. A decrease in pAkt was evidenced 30 minutes after stimulation in cells treated with the mentioned concentrations of ABP-09 (about 90-70% of the maximum pAkt response, Figure S13).

View Article Online
DOI: 10.1039/C8CP06196C

Physical Chemistry Chemical Physics

ARTICLE

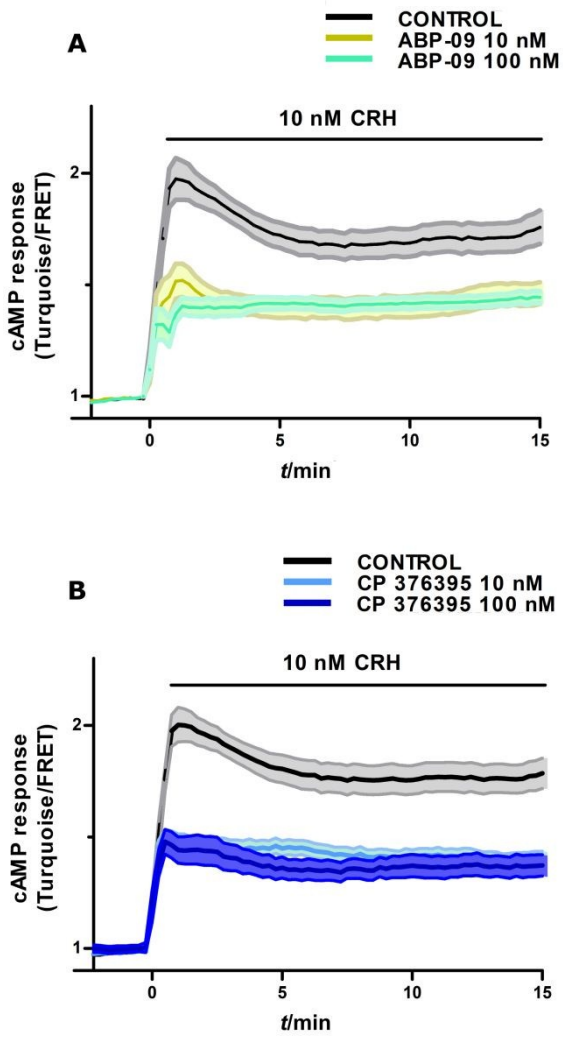

Figure 5. cAMP response measured by FRET in single HT22-CRHR1-Epac-SH187 cells, stimulated with 10 nM CRH at time 0 (mean ± SEM n= 14-25 cells) and preincubated with: A) ABP-09; B) CP-376395.

ABP-09 as a fluorescent probe for in vivo CRHR1 labeling and STORM imaging

The performance of ABP-09 was benchmarked against Alexa Fluor 647, one of the best-performing fluorophore for STORM. Two-color STORM imaging was performed in the HT22-CRHR1 cell line which expresses CRHR1 with a cMyc tag at the N-terminus (cMyc-CRHR1). Cells were treated with 10 nM ABP-09 during 20 h, fixed, and the cMyc tag was detected by indirect immunofluorescence using a specific anti-cMyc primary antibody and a secondary antibody labeled with Alexa Fluor 647 (Figure 6). The localization precision in single molecule localization depends on the width of the Point Spread Function (PSF) of the microscope, the pixel size of the detector, the number of photons collected per event, and the background noise.[58] High photon counts per frame favour location precision, while a low fraction of time in the on state allows location of the molecule in the presence of others as well as increases location speed.[59] Consequently, the brightness and blinking performance of ABP-09 was measured in comparison to Alexa Fluor 647. ABP-09 molecules show an average ON time of 33 ms compared to 35 ms for Alexa Fluor 647 (30 ms exposure time), while the ratio between photons emitted by Alexa Fluor 647 and ABP-09 molecules is 2.5 ± 0.5, both under incident laser excitation of (6 ± 1) $kW.cm^{-2}$ (see Figure S11). The photostability of ABP-09 is also comparable to Alexa Fluor 647. Images have a lateral localization precision of 26 ± 7 nm for Alexa Fluor 647, and 23 ± 7 nm for ABP-09 (Figure 6C). These results demonstrate the excellent features of ABP-09 as a probe for STORM. The slightly lower localization precision for Alexa Fluor 647 compared to ABP-09 in spite of the higher brightness of the former probe is attributed to two factors. The first one is the higher background observed in the Alexa Fluor 647 emission channel (Figure S11). The second one is the size (~10 nm) of the multiple fluorophore labelling of the secondary antibody. Instead, ABP-09 provides a true single molecule label to each receptor. The lower brightness of ABP-09 compared to Alexa Fluor 647 is explained by the lower absorption coefficient at the excitation wavelength: $7x10^4$ $M^{-1}cm^{-1}$ and 2.4 10^5 $M^{-1}cm^{-1}$, respectively. This brightness and stability places ABP-09 among the best performing dyes for single molecule localization in the green light excitation range.[59]

View Article Online
DOI: 10.1039/C8CP06196C

Physical Chemistry Chemical Physics

ARTICLE

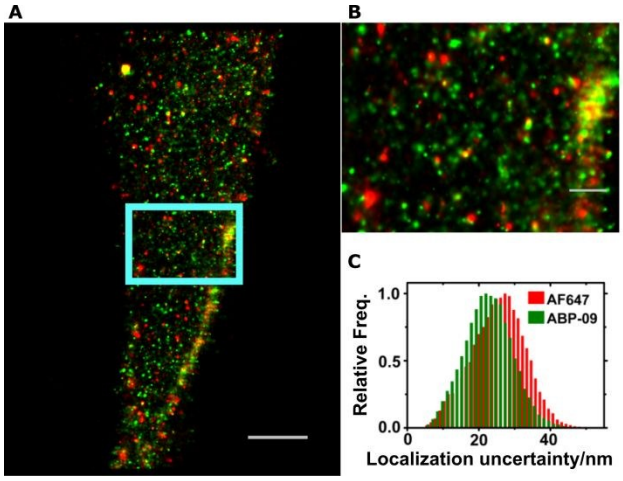

Figure 6. STORM images of labelled HT22-CRHR1 cells. Alexa Fluor 647 conjugated to antibodies (red channel) and ABP-09 (green channel). A) Whole cell image and B) Zoom in of the area marked in A. C) Histogram of the localization precision of single molecules for the two dyes. Scale bars: A) 2 μm; B) 500 nm.

Analysis of the molecular association between CRHR1 and ABP-09

Several methods have been reported to extract quantitative information of molecular association from fluorescence nanoscopy images, such as cluster distribution, pair correlation function, or point patterns, to statistically estimate significance in approach beyond the statistical random crowding.[60-66] Here we obtain an approximation to thermodynamic association equilibrium constants, by computing association coefficients $Q_{ij} = N_{ij}/(N_i.N_j)$, based on direct counting single and paired molecules (i,j representing either of the fluorophores). A comparison with simulated random distributions provides the reference and calibration of the method (see SI for detailed description). Figure 7A shows that the actual distributions, where HT22-CRHR1 cells were incubated for 20 h with 10 nM ABP-09, computed in different areas of various cells, always present greater association than that expected for random pairing. This result is in line with ABP-09 antagonistic effect on CRHR1 signaling. The effect of adding for 15 minutes the non-fluorescent CRHR1 antagonist CP-376395 in a large excess (10 and 100 μM) to HT22-CRHR1 cells incubated with 10 nM ABP-09, is also shown in Figure 7A. These last two curves match to a large extent and exhibit a lower fraction of ABP-09 / CRHR1 association events when compared to cells untreated with CP-376395. This observation confirms a displacement of ABP-09 from CRHR1 by the dark antagonist. Additionally, the indistinguishable behavior observed for the 10 and 100 μM CP-376395 treatments suggests that a complete displacement is achieved with the lower concentration tested. Figure 7B includes the analysis of the neighborhood between ABP-09 and CRHR1 in HT22 cells (not expressing cMyc-CRHR1) and compares it with the displacement experiments described for Panel A. The association observed in HT22 cells reflects both random pairing and unspecific binding of labeled antibodies and ABP-09. In both situations (HT22 cells and displacement experiments) the fraction of associated molecules was very similar and significantly lower than the one calculated from the experiments where HT22-CRHR1 cells were incubated with ABP-09 alone. This fact points out that CP-376395 and ABP-09 are competitors in the association to CRHR1, and that, after displacement, the residual association observed is due to random pairing and unspecific binding.

We should note that Q_{ab} includes pairs not only originated in molecular affinity but also others due to random neighborhood. Images show that ABP-09 and Alexa Fluor 647 also appear as self-associated (Figure 6). Therefore, we considered also the corresponding association constants to describe the molecular distribution of the whole system (see Figure S14 for Q_{aa} and Q_{bb}). The relation between Q_{ij} and their corresponding K_{ij} was explored by simulations of molecular distributions with different values of K_{ab}, K_{aa}, and K_{bb} as a function of molecular density. In these simulations Q_{ij} was computed and normalized to the corresponding random distribution ($Q_{ij,rndm}$, all $K_{ij} = 0$) with the same density, characterized by the parameter $R_{ab} = \log(Q_{ab}/Q_{ab,rndm})$. The results show that R_{ab} is constant to within ± 0.3 logarithmic units as a function of molecular density in a broad range of molecular density (Figure S15), providing a good calibration criterion.

From experimental data of Figure 7 we obtain $R_{ab} = 0.31 \pm 0.11$ (data of Figure 7 shown as logarithmic ratio in Figure S17). Assuming that $K_{aa} = K_{bb}$, due to the similar values of Q_{aa} and Q_{bb} (Figure S14), we obtain $\log K_{ab} = -4.1 \pm 0.2$, and $\log K_{aa} = \log K_{ab} = -3.2 \pm 0.2$. The observation volume of $1.35\ 10^9$ nm^3 was calculated considering the 200x200 pixels of 13x13 nm^2 area used as standard and an estimated TIRF irradiation depth of 200 nm. With it, $K_{ab} = 8\ 10^4$ M^{-1}; $K_{aa} = K_{bb} = 5\ 10^5$ M^{-1} are obtained. We will focus here in K_{ab}, as it represents the association between ABP-09 and CRHR1.

View Article Online
DOI: 10.1039/C8CP06196C

Physical Chemistry Chemical Physics

ARTICLE

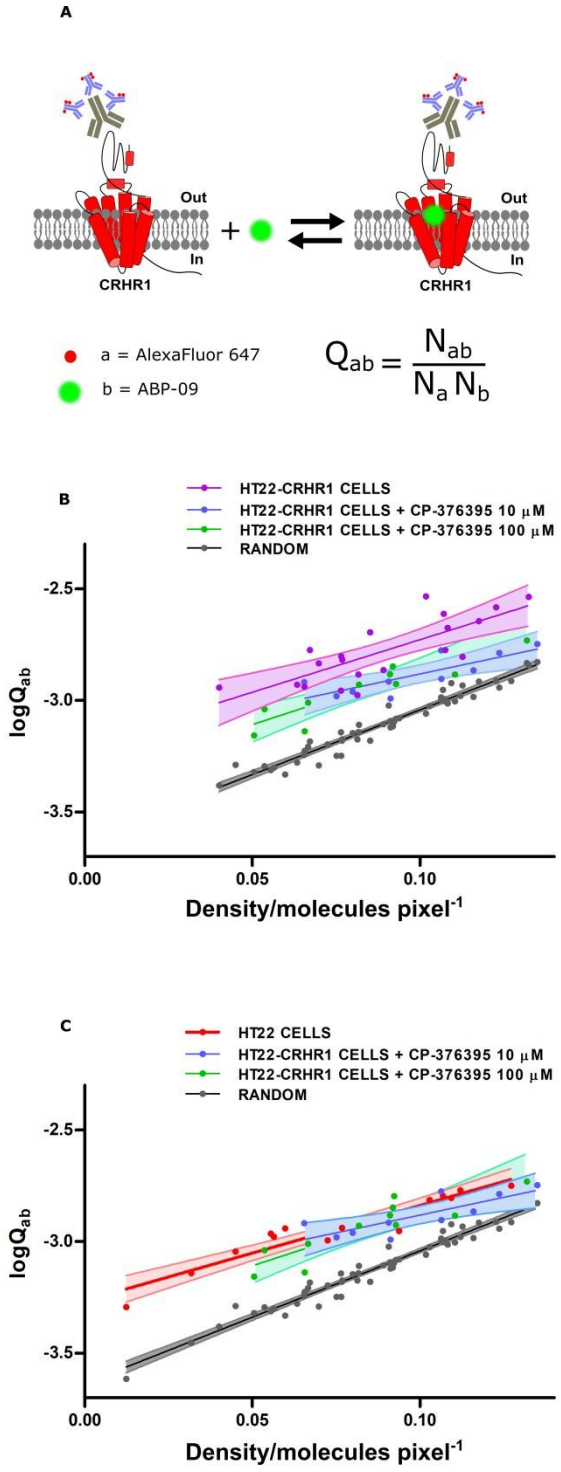

The dissociation constant of the ABP-09-CRHR1 complex (the inverse of K_{ab}) has a value of 12 μM. This value is around three orders of magnitude greater than those for potent CRHR1 antagonists.[31,32] Nevertheless, inhibition experiments demonstrate that ABP-09 and CP-376395 exert similar inhibiting cellular effects at the same nM bulk concentration range. The association constant we inform is obtained in a cell environment, where local concentration is higher than the average value of the concentration provided. More precisely, the average molecular density of around 0.1 molecules per pixel (the volume corresponding to a pixel is 13x13x200 nm^3) is equivalent to a concentration of 5 μM. It represents a 500-fold concentration increase compared to the 10 nM ABP-09 concentration added to the cell preparation to perform the experiments. Therefore, we can assess that the dissociation equilibrium constant of ABP-09-CRHR1 in bulk experiments would also lie in the nM range, as most potent known antagonists.

In reference to the value of the dissociation constant, some observations deserve consideration. In the first place, this estimation does not exclude from the analysis the possible unspecific binding of ABP-09 directly to labeled antibody. Experiments in HT22 cells could be an estimation of this fact, but this is not the only possible interpretation of these results (see below). Secondly, it considers each isolated ABP-09 or labeled antibody as free molecules, while they could also be associated to different cell components. Thus, these phenomena may result in an overestimation not only of molecular pairing, but also of the total number of free ABP-09 and/or CRHR1. Both effects tend to compensate.

Figure 7. A) Scheme of the association of ABP-09 to immunolabeled CRHR1 and definition of the pairing coefficient Q_{ab}. "a" stands for Alexa Fluor 647 and "b" stands for ABP-09. B) Plot of pairing coefficient Q_{ab} as a function of the average number of molecules per pixel in various regions of different HT22-CRHR1 cells treated with 10 nM ABP-09 (violet dots and curve; 3 cells, with 7, 7, and 6 areas examined) and for the same system after addition of 10 and 100 μM CP-376395 (blue and green dots/curves, respectively; 2 cells for each concentration, with 5 areas analyzed in each cell treated with 10 μM CP-376395, and 5 and 6 areas in the 100 μM CP-376395 condition). Black dots and curves represent the simulated distribution using the same molecular density as the experimental curves. C) Same as B) in HT22 cells treated with 10 nM ABP-09 (red dots and curve; 4 cells, with 2, 2, 4, and 6 areas considered). Green and blue dots/curves are the same as in panel B, while black curve corresponds to the respective reference random simulation. Shadowed regions show the 95% confidence interval of the linear fits.

View Article Online
DOI: 10.1039/C8CP06196C

Physical Chemistry Chemical Physics

ARTICLE

A further concern regards the coincidence of the results in HT22 cells and in HT22-CRHR1 cells displaced with CP-376395, as they systematically show a greater association than random simulations. If we assume that ABP-09 and CRHR1 are not associated to an appreciable extent in these experiments, the difference can be reasonably interpreted by assuming that the available space for CRHR1 and ABP-09 location does not correspond to the whole cell volume, as used in the simulations. Under this interpretation the available volume reduction results in a density increase that would shift horizontally in Figure 7C the lines corresponding to the experiments in HT22 cells and in HT22-CRHR1 cells displaced with CP-376395 with respect to the random simulations. If we perform this shift to make the curves coincide in Figure 7C, a factor of two can be estimated in the density.

We consider the reported value of the dissociation constant of ABP-09-CRHR1 to be robust because: i) the addition of CP-376395 as displacement agent decreases the association, measured by the parameter Q_{ab}, to levels similar to the ones in cells that lack cMyc tag, and that can therefore be taken as reference for unspecific association ii) as assessed by the molecular density in the field of view, concentrations lie in the μM range in the cell environment; iii) we observe variations in the fraction of associated and free molecules as a function of local concentration in different cell portions within this μM range.

Conclusions

The molecular design strategy used here, that combined molecular docking and photochemical stability criteria, proved successful in producing a fluorescent marker for the antagonist site of CRHR1. ABP-09, an aza-BODIPY, shows excellent emission properties for stochastic single molecule-based fluorescence nanoscopy. Structural information for other members of Class B GPCRs is currently growing. Thus, the strategy described in this work for the design of fluorescent probes based on known crystallographic structures anticipates a great impact in labeling experiments. In a wider sense, small molecule markers for proteins are suitable for tracking experiments in live cells, tissues, and even in whole organisms because this rationale avoids in-vitro fusion protein production. In addition, we have developed an analysis method that is broadly applicable, to estimate association constants from high resolution localization microscopy images in cells.

Experimental Section

***Computational chemistry*.**

All simulations were based on the crystal structure of Class B GPCR CRHR1.[3] The molecular system was described in the dihedral space using the ECEPP/3 force field[67,68] within the ICM program[36,37] and prepared in a similar fashion as in earlier works.[69-71] Docking was performed within the orthosteric binding site after deleting all water molecules and co-factors, using a flexible-ligand—rigid-receptor approach as implemented in ICM. In the docking algorithm the torsional degrees of freedom (DOF) of the small-molecules and their six rigid coordinates were considered flexible within the receptor energy field, and subjected to a Monte Carlo global energy minimization. On the lowest docking energy pose of each molecule an empirical docking score was calculated according to its fit within the binding site.[72] To improve convergence of the global energy minimization step, docking was performed twice and the lowest score per molecule was kept. Docked structures were refined in a ligand-steered fashion, where the molecules' DOF and receptor side chains within 6.0 Å were optimized using an energy minimization protocol (for a detailed description cf. Refs.[41,43,73]).

Synthesis of ABP-09.

The synthetic procedures and characterization of ABP-09 and intermediate compounds **1**, **2**, and **3** (Figure 3) is described in the SI. The synthesis has been adapted from reported procedures. Characterization of final product and reaction intermediates was achieved by combination of analytical, spectroscopic, and spectrometric procedures (Figures S1-S7). Spectral characterization of ABP-09 was carried out by absorption spectroscopy, and steady state and time resolved fluorescence spectroscopy, as detailed in the SI.

***ABP-09 uptake in live cells*.**

HT22-CRHR1 cells were incubated in phenol red free DMEM low glucose (Invitrogen) supplemented with 20 mM Hepes, 26 mM $NaHCO_3$ and 10 nM or 100 nM of ABP-09. Fluorophore uptake kinetics in live cells was measured for 24 h using widefield fluorescence microscopy. Cell imaging conditions and fluorescence quantification protocols are described in the SI. In Figure S12 the temporal evolution of emission arising from live cells is shown. From these

View Article Online
DOI: 10.1039/C8CP06196C

Physical Chemistry Chemical Physics

ARTICLE

experiments, we selected a 20 h preincubation time for ABP-09 when used in cells.

Spectral FRET and imaging of cAMP.

HT22-CRHR1-Epac-S^{H187} cells were preincubated as described for HT22-CRHR1 cells in ABP-09 uptake experiments. To study the effect of CP-376395 (3212, TOCRIS), preincubation was carried in either 10 or 100 nM concentration of this compound. For control cells DMSO (vehicle) was used in the 20 h preincubation event. FRET experiments were carried out as previously described.[56] The acquisition conditions, image processing protocols and the characteristics of the fluorescence microscope are reported in detail in the SI. Briefly, HT22-CRHR1-EPAC-S^{H187} cells were seeded in glass-bottom dishes, grown, and incubated with ABP-09, CP-376395 or DMSO, as previously described. After preincubation, cells were stimulated with 10 nM of human/rat CRH (H-2435, Bachem) at time 0. Movies were recorded acquiring images every 15 s, from t = -2 min until t = 15 min, at the spectral channels corresponding to the FRET pair (mTurquoise2 and Venus) and to ABP-09.

Super-resolution fluorescence microscopy (STORM).

For STORM microscopy, HT22-CRHR1 and HT22 cells were preincubated for 20 h in phenol red free DMEM low glucose (Invitrogen) supplemented with 20 mM Hepes, 26 mM $NaHCO_3$ and 10 nM ABP-09. For the antagonist displacement analysis, after the preincubation with ABP-09, cells were incubated 15 min with 10 μM or 100 μM CP-376395. Fixation, immunolabeling protocol and coverslip cleaning are described in detail in the SI. The STORM microscope was custom-built around an Olympus IX-73 inverted microscope operating in wide-field epifluorescence mode (Figure S8). Two color images were acquired with an oil immersion objective Olympus PlanApo 60x NA 1.42. Total internal reflection illumination mode (TIRF) was enabled by moving a linear stage (Thorlabs) so that the focus of the lasers translated laterally within the back focal plane of the objective. Fluorescent emission from different species were separated with a dichroic mirror (Chroma ZT647rdc) and imaged onto adjacent areas of the EMCCD camera (Andor iXon3 897). The camera and lasers were controlled with custom software developed in the laboratory and described in an earlier publication.[74] A more extensive description of the microscope components can be found in the SI and Figure S8. The calibration protocol to find the affine transformation matrix for optimally overlapping the two emission channels is also presented in the SI. STORM data acquisition was carried out under laser intensities of 5-10 kW cm^{-2} for excitation, thus inducing on-off switching of the fluorescent markers in the tens of ms time range, as required by the STORM technique. A Pre-Amp Gain of 5.1 and an EM Gain of 40 were used in the CCD camera. Throughout the whole acquisition, the activation 405 nm laser power was increased in steps whenever the density of single-molecule events decreased below ~1 molecule per μm^2. Typically, it took 20,000 frames of 30 ms of exposition time for each STORM acquisition. The previously found affine transformation was then applied to the raw images. Subsequent data analysis and the rendering of the final super-resolved image were performed with ThunderSTORM software[75] and finally the two color images were assembled with ImageJ/Fiji.[76]

Estimation of the CRHR1-ABP-09 binding constant.

STORM images were processed with a 13.3 nm pixel size to locate the molecules. For the assessment of association, a 9 pixel pattern was considered: the pixel where the central molecule was located and the 8 surrounding ones. Single molecule locations in a reconstructed STORM image were analyzed with custom MATLAB routines to count molecular pairs and isolated molecules. In this way Q_{ij} values are computed. To translate them into K_{ij} values, simulated distributions for the random case and for different sets of values of K_{ij} as a function of molecular density were used to calculate the ratio $Q_{ab}/Q_{ab,rndm}$ in each case (FigureS15 for the simulations and FigureS17 for HT22-CRHR1 cells). The density-averaged value of $R_{ab} = \log(Q_{ab}/Q_{ab,rndm})$ was plotted as a function of input values of the K_{ij} (FigureS16) to render the final calibration from which association constants can be estimated.

Conflicts of interest

There are no conflicts to declare.

Acknowledgements

FDS, SEB, LG, CNC, SS, and PFA are Research Staff from CONICET (Consejo Nacional de Investigaciones Científicas y Técnicas, Argentina). AMS and FMB hold research

View Article Online
DOI: 10.1039/C8CP06196C

Physical Chemistry Chemical Physics

ARTICLE

fellowships from CONICET, and NGA, a fellowship from Agencia Nacional de Promoción Científica y Tecnológica (ANPCyT). This work was supported by grants PICT2011-2778, PICT2014-3599, PICT2013-1931, PICT2013-MP0392 (ANPCyT), PIP0397 and 0626 from CONICET, and grant from Fondo para la Convergencia Estructural del Mercosur (COF 03/11). CNC thanks Molsoft LLC for providing an academic license for the ICM program. The authors thank the National System of High Performance Computing (Sistema Nacional de Computación de Alto Rendimiento, SNCAD) and the Computational Centre of High Performance Computing (Centro de Computación de Alto Rendimiento, CeCAR) for granting use of their computational resources.

Notes and references

1 A. Bortolato, A. S. Dore, K. Hollenstein, B. G. Tehan, J. S. Mason, F. H. Marshall, *Br. J. Pharmacol.* 2014, **171**, 3132.
2 T. P. Sakmar, *Chem. Rev.* 2017, **117**, 1.
3 K. Hollenstein, J. Kean, A. Bortolato, R. K. Cheng, A. S. Dore, A. Jazayeri, R. M. Cooke, M. Weir, F. H. Marshall, *Nature* 2013, **499**, 438.
4 F. Y. Siu, M. He, C. de Graaf, G. W. Han, D. Yang, Z. Zhang, C. Zhou, Q. Xu, D. Wacker, J. S. Joseph, W. Liu, J. Lau, V. Cherezov, V. Katritch, M. W. Wang, R. C. Stevens, *Nature* 2013, **499**, 444.
5 E. R. de Kloet, M. Joels, F. Holsboer, *Nat. Rev. Neurosci.* 2005, **6**, 463.
6 E. W. Hillhouse, D. K. Grammatopoulos, *Endocr. Rev.* 2006, **27**, 260.
7 C. Inda, N. G. Armando, P. A. dos Santos Claro, S. Silberstein, *Endocr. Connect*. 2017, **6**, R99.
8 M. Paez-Pereda, F. Hausch, F. Holsboer, *Exper. Opin. Investig. Drugs* 2011, **20**, 519.
9 J. Sanders, C. Nemeroff, *Trends Pharmacol. Sci.* 2016, **37**, 1045.
10 S. W. Hell, Nobel Lecture: Nanoscopy with focused light. Dec. 8, 2014,
11 S. W. Hell, J. Wichmann, *Opt. Lett.* 1994, **19**, 780.
12 E. Betzig, Nobel Lecture: Single Molecule, Cells and Super-Resolution Optics. Dec. 8, 2014,
13 P. F. Aramendía, M. L. Bossi, in Far-Field Optical Nanoscopy (Eds: P. Tinnefeld, C. Eggeling, S. W. Hell), Springer, Berlin Heidelberg, Germany 2012, pp 189-213.
14 G. Patterson, M. Davidson, S. Manley, J. Lippincott-Schwartz, *Annu. Rev. Phys. Chem*. 2010, **61**, 345.
15 F. Balzarotti, Y. Eilers, K. C. Gwosch, A. H. Gynna, V. Westphal, F. D. Stefani, J. Elf, S. W. Hell, *Science* 2017, **355**, 606.
16 M. J. Hinner, K. Johnsson, *Curr. Opin. Biotechnol.* 2010, **21**, 766.
17 Y. Hori, K. Kikuchi, *Curr. Opin. Chem. Biol.* 2013, **17**, 644.
18 B. A. Griffin, S. R. Adams, R. Y. Tsien, *Science* 1998, **281**, 269.
19 A. Keppler, S. Gendreizig, T. Gronemeyer, H. Pick, H. Vogel, K. Johnsson, *Nat. Biotechnol*. 2003, **21**, 86.
20 Y. Ishitsuka, N. Azadfar, A. Y. Kobitski, K. Nienhaus, N. Johnsson, G. U. Nienhaus, *J. Phys. Chem. B.* 2015, **119**, 6611.
21 T. Kowada, H. Maeda, K. Kikuchi, *Chem. Soc. Rev.* 2015, **44**, 4953.
22 J. A. Hern, A. H. Baig, G. I. Mashanov, B. Birdsall, J. E. Corrie, S. Lazareno, J. E. Molloy, N. J. Birdsall, *Proc. Natl. Acad. Sci. U S A* 2010, **107**, 2693.
23 M. Zhao, L. Du, M. Li, *J. Med. Chem*. 2014, 57, 8187-8203.
24 A. D. Stumpf, C. Hoffmann, *Br. J. Pharmacol.* 2016, **173**, 255.
25 J. Azuaje, P. Lopez, A. Iglesias, R. A. de la Fuente, J. M. Perez-Rubio, D. Garcia, T. M. Stepniewski, X. Garcia-Mera, J. M. Brea, J. Selent, D. Perez, M. Castro, M. I. Loza, E. Sotelo, *Sci. Rep.* 2017, **7,** 10765.
26 H. Tian, A. Furstenberg, T. Huber, *Chem. Rev.* 2017, **117**, 186.
27 M. Schonberger, D. Trauner, *Angew. Chem.* 2014, **126**, 3329; *Angew. Chem. Int. Ed. Engl.* 2014, **53**, 3264.
28 J. Broichhagen, N. R. Johnston, Y. von Ohlen, H. Meyer-Berg, B. J. Jones, S. R. Bloom, G. A. Rutter, D. Trauner, D. J. Hodson, *Angew. Chem.* 2016, **128,** 5961; *Angew. Chem. Int. Ed. Engl.* 2016, **55**, 5865.
29 P. C. Donthamsetti, N. Winter, M. Schonberger, J. Levitz, C. Stanley, J. A. Javitch, E. Y. Isacoff, D. Trauner, *J. Am. Chem. Soc.* 2017, **139**, 18522.
30 L. Agnetta, M. Kauk, M. C. A. Canizal, R. Messerer, U. Holzgrabe, C. Hoffmann, M. Decker, *Angew. Chem*. 2017, **129**, 7388; *Angew. Chem. Int. Ed. Engl.* 2017, **56**, 7282.
31 B. A. Fleck, S. R. Hoare, R. R. Pick, M. J. Bradbury, D. E. Grigoriadis, *J. Pharmacol. Exp. Ther.* 2012, **341**, 518-531.
32 Y. L. Chen, R. S. Obach, J. Braselton, M. L. Corman, J. Forman, J. Freeman, R. J. Gallaschun, R. Mansbach, A. W. Schmidt, J. S. Sprouse, F. D. Tingley Iii, E. Winston, D. W. Schulz, *J. Med. Chem*. 2008, **51**, 1385.
33 C. Devigny, F. Perez-Balderas, B. Hoogeland, S. Cuboni, R. Wachtel, C. P. Mauch, K. J. Webb, J. M. Deussing, F. Hausch, *J. Am. Chem. Soc.* 2011, **133**, 8927.
34 A. Loudet, K. Burgess, Chem. Rev. 2007, 107, 4891.
35 G. Ulrich, R. Ziessel, A. Harriman, *Angew. Chem.* 2008, **120**, 1202; *Angew. Chem. Int. Ed. Engl.* 2008, **47**, 1184.
36 ICM, Version 3.7.2; MolSoft, LLC: La Jolla, CA, 2012.
37 R. Abagyan, M. Totrov, D. Kuznetsov, *J. Comp. Chem*. 1994, **15**, 488.
38 D. Wootten, J. Simms, L. J. Miller, A. Christopoulos, P. M. Sexton, *Proc. Natl. Acad. Sci. U S A* 2013, **110**, 5211.
39 C. N. Cavasotto, in Physico-Chemical and Computational Approaches to Drug Discovery (Eds: F. J. Luque, X. Barril), Royal Society of Chemistry, London, UK 2012; pp 195-222.
40 F. Spyrakis, C. N. Cavasotto, *Arch. Biochem. Biophys.* 2015, **583**, 105.

View Article Online
DOI: 10.1039/C8CP06196C

Physical Chemistry Chemical Physics

ARTICLE

41 C. N. Cavasotto, A. J. Orry, N. J. Murgolo, M. F. Czarniecki, S. A. Kocsi, B. E. Hawes, K. A. O'Neill, H. Hine, M. S. Burton, J. H. Voigt, R. A. Abagyan, M. L. Bayne, F. J. Monsma, Jr., *J. Med. Chem.* 2008, **51**, 581.
42 R. R. Petrov, L. Knight, S. R. Chen, J. Wager-Miller, S. W. McDaniel, F. Diaz, F. Barth, H. L. Pan, K. Mackie, C. N. Cavasotto, P. Diaz, Eur. *J. Med. Chem.* 2013, **69**, 881-907.
43 S. S. Phatak, E. A. Gatica, C. N. Cavasotto, *J. Chem. Inf. Model.* 2010, **50**, 2119.
44 D. Wu, D. F. O'Shea, *Org. Lett.* 2013, **15**, 3392.
45 M. Grossi, A. Palma, S. O. McDonnell, M. J. Hall, D. K. Rai, J. Muldoon, D. F. O'Shea, *J. Org. Chem*. 2012, **77**, 9304.
46 A. Loudet, R. Bandichhor, L. Wu, K. Burgess, *Tetrahedron* 2008, **64**, 3642.
47 M. Strobl, T. Rappitsch, S. M. Borisov, T. Mayr, I. Klimant, *Analyst* 2015, **140**, 7150.
48 G. Fan, L. Yang, Z. Chen, *Front. Chem. Sci. Eng.* 2014, **8**, 405.
49 A. Kamkaew, S. H. Lim, H. B. Lee, L. V. Kiew, L. Y. Chung, K. Burgess, *Chem. Soc. Rev.* 2013, **42**, 77.
50 J. H. Gibbs, L. T. Robins, Z. Zhou, P. Bobadova-Parvanova, M. Cottam, G. T. McCandless, F. R. Fronczek, M. G. Vicente, *Bioorg. Med. Chem.* 2013, **21**, 5770.
51 J. K. Karlsson, A. Harriman, *J. Phys Chem. A.* 2016**, 120**, 2537.
52 A. Gut, L. Lapok, D. Jamróz, A. Gorski, J. Solarski, M. Nowakowska, *New J. Chem.* 2017**, 41**, 12110.
53 F. López Arbeloa, J. Banuelos Prieto, V. Martínez Martínez, T. López Arbeloa, I. López Arbeloa, *ChemPhysChem* 2004**, 5**, 1762.
54 V. Leen, D. Miscoria, S. Yin, A. Filarowski, J. M. Ngongo, M. Van der Auweraer, N. Boens, W. Dehaen, *J. Org. Chem.* 2011**, 76**, 8168.
55 W. Qin, V. Leen, T. Rohand, W. Dehaen, P. Dedecker, M. Van der Auweraer, K. Robeyns, L. Van Meervelt, D. Beljonne, B. Van Averbeke, J. N. Clifford, K. Driesen, K. Binnemans, N. Boens, *J. Phys. Chem. A.* 2009**, 113**, 439.
56 C. Inda, P. A. dos Santos Claro, J. J. Bonfiglio, S. A. Senin, G. Maccarrone, C. W. Turck, S. Silberstein, *J. Cell. Biol.* 2016, **214**, 181.
57 C. Inda, J. J. Bonfiglio, P. A. dos Santos Claro, S. A. Senin, N. G. Armando, J. M. Deussing, S. Silberstein, *Sci. Rep.* 2017, **7,** 1944.
58 R. E. Thompson, D. R. Larson, W. W. Webb. *Biophys. J.* 2002, **82**, 2775.
59 G. T. Dempsey, J. C. Vaughan, K. H. Chen, M. Bates, X. Zhaung. *Nature Meth.* 2011, **8**, 1027.
60 W. Vandenberg, M. Leutenegger, T. Lasser, J. Hofkens, P. Dedecker, *Cell Tissue Res.* 2015, **360**, 151.
61 P. R. Nicovich, D. M. Owen, K. Gaus, *Nat. Protoc.* 2017, **12**, 453.
62 K. W. Dunn, M. M. Kamocka, J. H. McDonald, *Am. J. Physiol. Cell. Physiol.* 2011, **300**, 723.
63 J. Rossy, E. Cohen, K. Gaus, D. M. Owen, *Histochem. Cell. Biol.* 2014, **141**, 605.
64 K. Bermudez-Hernandez, S. Keegan, D. R. Whelan, D. A. Reid, J. Zagelbaum, Y. Yin, S. Ma, E. Rothenberg, D. Fenyo, *Sci. Rep.* 2017, **7**, 14882.
65 E. Sherman, V. A. Barr, L. E. Samelson, *Methods* 2013, **59**, 261.
66 P. Rubin-Delanchy, G. L. Burn, J. Griffie, D. J. Williamson, N. A. Heard, A. P. Cope, D. M. Owen, *Nat. Methods* 2015, **12**, 1072.
67 G. Nemethy, K. D. Gibson, K. A. Palmer, C. N. Yoon, M. G. Paterlini, A. Zagari, S. Rumsey, H. A. Scheraga, *J. Phys. Chem.* 1992, **96**, 6472.
68 R. Abagyan, M. Totrov, *J. Mol. Biol.* 1994, **235**, 983.
69 C. S. Brand, H. J. Hocker, A. A. Gorfe, C. N. Cavasotto, C. W. Dessauer, *J. Pharmacol. Exp. Ther*. 2013, **347**, 265.
70 E. S. Leal, M. G. Aucar, L. G. Gebhard, N. G. Iglesias, M. J. Pascual, J. J. Casal, A. V. Gamarnik, C. N. Cavasotto, M. Bollini, *Bioorg. Med. Chem. Lett.* 2017, **27**, 3851
71 M. J. Pascual, F. Merwaiss, E. Leal, M. E. Quintana, A. V. Capozzo, C. N. Cavasotto, M. Bollini, D. E. Alvarez, *Antiviral Res*. 2018, **149**, 179.
72 M. Totrov, R. Abagyan, in Drug-receptor thermodynamics: Introduction and experimental applications, (Ed: R. B. Raffa), John Wiley & Sons, New York, USA 2001, pp 603-624.
73 C. N. Cavasotto, M. G. Aucar, N. S. Adler, *Int. J. Quantum. Chem*. 2018, in press DOI: 10.1002/qua.2678.
74 F. M. Barabas, L. A. Masullo, F. D. Stefani, *Rev. Sci. Instr.* 2016, **87**, 126103.
75 M. Ovesny, P. Krizek, J. Borkovec, Z. Svindrych, G. M. Hagen, *Bioinformatics* 2014, **30**, 2389.
76 J. Schindelin, I. Arganda-Carreras, E. Frise, V. Kaynig, M. Longair, T. Pietzsch, S. Preibisch, C. Rueden, S. Saalfeld, B. Schmid, J. Y. Tinevez, D. J. White, V. Hartenstein, K. Eliceiri, P. Tomancak, A. Cardona, *Nat. Methods* 2012, **9**, 676.